Magnetic Resonance Materials in Physics, Biology and Medicine (2019) 32:501–509
https://doi.org/10.1007/s10334-019-00745-3

RESEARCH ARTICLE

Chemotherapy response of pancreatic cancer by diffusion-weighted imaging (DWI) and intravoxel incoherent motion DWI (IVIM-DWI) in an orthotopic mouse model

Li Wu[1,2] · Jing Li[3] · Caixia Fu[4] · Bernd Kühn[5] · Xiaolin Wang[6,7]

Received: 8 August 2018 / Revised: 19 January 2019 / Accepted: 17 February 2019 / Published online: 1 March 2019

Abstract

Purpose To investigate the value of using diffusion-weighted imaging (DWI) and intravoxel incoherent motion DWI (IVIM-DWI) to assess the chemotherapy response of pancreatic cancer in an orthotopic mouse model.

Materials and methods Twenty-four BALB/C nu/nu mice in two groups ($n=12$/group) with human pancreatic adenocarcinoma xenografts were dosed intravenously with saline (group 1) and gemcitabine (group 2). DWI with 3 b values ($b=50$, 400 and 800 s/mm^2) and IVIM-DWI with multiple b values ($b=0$, 25, 50, 80, 100, 300, 500, 800 s/mm^2) were performed on the day before and 1 and 10 days after the treatment. Regions of interest (ROI) were drawn and tumor ADC, D_{slow}, D_{fast} and f_p values derived from the DWI and IVIM-DWI were compared between the two groups. At the day 28 after the treatment, the tumors were harvested for histologic analyses.

Results The values of ADC and D_{slow} in the entire tumor region were significantly increased in gemcitabine-treated group in contrast to saline-untreated group at day 1 ($1.88\pm0.34\times10^{-3}$ s/mm^2 vs $1.45\pm0.16\times10^{-3}$ s/mm^2, $P=0.028$, and $1.74\pm0.29\times10^{-3}$ s/mm^2 vs $1.34\pm0.26\times10^{-3}$ s/mm^2, $P=0.030$), but D_{fast} and f_p values were not significantly different. Immunohistochemical results showed that cell proliferation was significantly reduced ($P<0.001$) and cell apoptosis ($P<0.001$) significantly increased in gemcitabine group compared to saline group. MVD was not significantly different.

Conclusion Both ADC value and D_{slow} value can be used as early imaging marker to assess the early chemotherapy response of pancreatic cancer.

Keywords Pancreatic cancer · Diffusion-weighted MRI (DWI) · Intravoxel incoherent motion · (IVIM)

✉ Li Wu
fdwl525@163.com

1 Institute of Biomedical Manufacturing and Life Quality Engineering, School of Mechanical Engineering, Shanghai Jiao Tong University, 800 Dongchuan Road, Shanghai, China

2 Department of Radiology, Zhongshan Hospital, Fudan University, Shanghai, China

3 Institute of Diagnostic and Interventional Radiology, Shanghai Jiao Tong University Affiliated Sixth People's Hospital, Shanghai, China

4 MR Application Development, Siemens Shenzhen Magnetic Resonance Ltd, Shenzhen, China

5 MR Application Predevelopment, Siemens Healthcare, Erlangen, Germany

6 Shanghai Institute of Medical Imaging, Shanghai, China

7 Department of Interventional Radiology, Zhongshan Hospital, Fudan University, Shanghai, China

Introduction

Pancreatic cancer remains one of the most life-threatening malignancies in the world. Statistics by the American Cancer Society shows that 53,670 new cases of pancreatic cancer were diagnosed in 2017 and 43,090 will die from the disease [1]. Most pancreatic cancers do not present early specific sign and symptoms and are usually diagnosed at the very advanced stage with distant metastasis to other organs. Consequently, the majority of patients diagnosed with pancreatic cancers are unresectable [2]. Gemcitabine-based chemotherapy has been accepted as the first line of treatment for the patients with advanced pancreatic cancers [3]. However, the current work revealed that gemcitabine therapy caused different efficacy [4, 5], so it is highly desirable to develop a reliable technique to evaluate the early response to chemotherapy, which is essential for optimizing the regimen.

Nowadays, the development of advanced imaging technique has been emerging as the most widely used non-invasive technique for evaluating the response of tumors to therapies [6–9]. Diffusion-weighted (DW) imaging modality is sensitive to the random Brownian motion of free water molecules and is quantified by the calculation of apparent diffusion coefficients (ADCs). It has been increasingly used for assessing the therapeutic effect of treatments in tumors [10, 11]. However, ADC values are influenced by both tissue diffusivity and pseudorandom motion caused by microcapillary perfusion, also known as pseudodiffusion [12].

The intravoxel incoherent motion (IVIM) model, separate measurement of the perfusion-related parameters at low b values (pseudodiffusion coefficient D_{fast} and the pseudodiffusion factor f_p) and the pure molecular-based diffusion coefficient D_{slow} at b values higher than 100 s/mm^2 can also be obtained with biexponential fitting of the signal intensity versus b curve using multi-b DWI [13–15]. This advanced imaging technique has been shown to be useful for the evaluation of treatment response to nasopharyngeal carcinoma, hepatocellular carcinoma, breast cancer liver metastases, and others [16–18]

The main mechanism of gemcitabine is to inhibit cell proliferation and promote apoptosis in pancreatic cancer cells [19]. Based on this mechanism, the number of tumor cells can be reduced and the diffusion of water molecules can be accelerated so there would be anticipated change in the diffusion-related coefficient compared to perfusion-related coefficient when using gemcitabine. In this study, we used diffusion-weighted imaging (DWI) and intravoxel incoherent motion DWI (IVIM-DWI) to assess the chemotherapy response of pancreatic cancer in an orthotopic mouse model to prove our hypotheses.

Materials and methods

Animals and animal model with orthotopic pancreatic cancer

All the experimental protocols were approved by the Ethics Committee of Shanghai Jiao Tong University (Approval no. 201801013) and were conducted in strict accordance with the Guidelines of the National Institutes of Health for the Care and Use of Laboratory Animals. Twenty-four male BALB/C nu/nu mice (5 weeks old, 15–17 g body weight) were used for creating orthotopic pancreatic cancer model.

The human pancreatic adenocarcinoma cell line SW1990 was purchased from American Type Culture Collection (ATCC). The mice were anesthetized with 100 µl of 2% pentobarbital sodium injected into the abdominal cavity. Then the abdominal cavity was opened by a 5–10-mm transverse incision on the left flank. The tail of the pancreas was exposed through this incision. Tumor cells (2×10^6) were inoculated in the joint portion between the body and tail of the pancreas.

DW MRI and IVIM DWI of the tumors

Twenty-four mice with pancreatic cancers were randomly allocated to two groups after 1 week of inoculation. Twelve mice were treated with gemcitabine and twelve mice were treated with saline as a control. Gemcitabine was intravenously administrated to the mice at a dose of 50 mg/kg once a week for 3 weeks and then 1 week interval without chemotherapy. MRI was performed 1 day prior to the administration of the first dose of gemcitabine (Day −1), 1 day after the first dose of gemcitabine (Day 1) and 10 days after the initiation of the therapy (Day 10). MR imaging was performed on a 1.5-Tesla MR scanner (MAGNETOM Aera, SIEMENS Healthcare, Erlangen, Germany) with a 16-channel Hand/Wrist coil (SIEMENS Healthcare, Erlangen, Germany). Mice were anesthetized with intraperitoneal injection with 100 µl of 2% pentobarbital sodium, and to minimize the distortion artifact in echo planar images, mice were kept in 37.0 ± 0.2 °C water in a plastic box with only head outside of the water for breathing during the MR scanning.

First, transverse and coronal MR images of the upper abdomen were acquired, including T2-weighted fast spin echo images, and free-breathing routine DW echo planar images with three b values (b = 50, 400 and 800 s/mm^2) for ADC measurement. Second, free-breathing multi-b DW MRI (b = 0, 25, 50, 80, 100, 300, 500, 800 s/mm^2) for IVIM measurement were acquired. The routine 3-b DWI sequence has its own advantage of shorter scanning time and less motion sensitivity, while IVIM sequence acquires more b values, needs longer scanning time and might be more motion-sensitive. Using ADC generated from the subset b values of the IVIM sequence might underestimate the performance of the conventional ADC. Thus, we use two separated sequences to acquired ADC and IVIM. Details regarding all sequence parameters are summarized in Table 1.

MR imaging analysis

Tumor volume was calculated using the formula for ellipsoid tumors, $V = L\times W\times D\times(\pi/6)$, where L and W are the largest length and width measured on the coronal image, D represents the largest depth measured on the axial image [20].

ADC maps were generated from DW images at b = 50,400 and 800 s/mm^2 automatically using the Syngo software (SIEMENS Healthcare, Erlangen, Germany), and IVIM-derived maps were generated using a prototype post-processing program integrated in Syngo software (SIEMENS Healthcare, Erlangen, Germany).

Table 1 Parameters of the MR sequences

Parameters	T_2WI (coronal)	T_2WI (transversal)	DWI	IVIM
Sequence	TSE	TSE	EPSE	EPSE
TR/TE (ms)	4070/78	5170/78	4100/88	4100/88
FOV (mm)	160	160	160	160
Slice thickness(mm)	1.5	1.5	1.3	1.3
Imaging matrix	320×240	448×358	128×128	128×128
Flip angle (°)	150	150		
Voxel size (mm)	0.5×0.5×1.5	0.4×0.4×1.5	1.3×1.3×1.3	1.3×1.3×1.3
Bandwidth (Hz/pixel)	191	189	1220	1220
Total measure time (min:s)	2:36	2.11	2: 15	4:39

T2WI T2-weighted imaging, *DWI* diffuse weighted imaging, *IVIM* intravoxel incoherent motion, *TSE* turbo spin echo, *EPSE* echo plana

The ADC values were calculated by fitting the signal intensity to a mono-exponential model as: $S(b) = S_0 \exp(-b\mathrm{ADC})$, where $S(b)$ is the signal intensity with a given b value and S_0 is the signal intensity without diffusion weighting [21]. For IVIM-derived parameter maps, a biexponential model was used for the calculation of the molecular diffusion-related coefficient D_{slow}, pseudodiffusion coefficient D_{fast}, and the pseudodiffusion fraction f_p as follows [22] :

$$S(b) = S_0\left(f_p \exp\left(-b\left(D_{fast} + D_{slow}\right)\right) + \left(1 - f_p\right)\exp\left(-bD_{slow}\right)\right)$$

To generate three parametric images (D_{slow}, D_{fast} and f_p), the above biexponential model was fit using the following approach: initial estimation of D_{slow} using a reduced set of b values larger than a predetermined value (200 s/mm^2) and then using the resulting D_{slow} as a fix parameter to fit the missing parameters similar to what was described in [22].

ROIs were manually drawn to encompass the entire tumor area on DW images with $b = 800$ s/mm^2 by two image reviewers (an MRI physicist and an abdominal radiologist, with 7 and 5 years of experience in abdomen MR imaging, respectively). Then ROIs were copied to ADC maps and three IVIM-derived parametric maps. For each ROI, mean values were calculated by Syngo software on each parametric map.

Histology

The mice were euthanized for harvesting the tumor at day 28. Tumors were fixed in 10% buffered formalin and were cut in half before embedding in paraffin. The halves were processed separately, with the cut edge ultimately facing the microtome surface. Serial 4 μm-thick sections were cut on a rotary microtome. Sections were deparaffinized in xylene and washed in gradient alcohol.

For Ki67 and VEGF staining, the sections were incubated in 3% hydrogen peroxide (H_2O_2) for 15 min for endogenous peroxidase activity blockade and heated in an autoclave in citrate buffer (pH 6.0) for 10 min for antigen retrieval, followed by blocking non-specific antigen with 10% normal goat serum (NGS) for 1 h, then the sections were incubated with the primary antibody against CD31 and Ki67 (abcam, Abcam Hong Kong Ltd, China) overnight at 4 °C. HRP-linked anti-rabbit/mouse antibodies (EnViSion Detection Kit, Gene Tech company, China) were used as secondary antibodies,

For TUNEL staining, incubate tissue sections for 15 min at 37 °C with proteinase K working solution, followed by which add 50 μl TUNEL reaction mixture for 60 min at 37 °C in a humidified atmosphere in the dark, then the sections were incubated in a humidified chamber for 60 min at 37 °C with 50 μl Converter-POD.

All tissue sections were developed using diaminobenzidine (DAB) as the chromogen and counterstained with hematoxylin, dehydrated, and cover-slipped. Obvious vascular endothelial cell coloring marked with CD31 and nucleus coloring marked with Ki67 were determined positive. The counting method described by Mehta et al. [23] was adapted for evaluation of MVD and Ki67 expression. Apoptotic cell number was also calculated.

Statistical analysis

Quantitative variables were presented as mean ± SEM. We performed statistical analysis using the statistical software SPSS (SPSS version 16.0, IBM Corporation, New York, USA). the Kolmogorov–Smirnov test was used to determine if the data have a normal distribution. Normally distributed variables were analyzed using independent Student's t test. For the data which were not normally distributed, the nonparametric Mann–Whitney sum rank test was used to compare the difference. For all statistical analyses, a P value less than 0.05 was considered to indicate a significant difference.

Results

MRI findings

The T_2WI and representative parameter maps of orthotopic pancreatic tumor were successfully obtained with minimal motion artifact (Fig. 1). To study the size of tumors, high-resolution T_2WI in the coronal and transverse planes were analyzed. Tumors could be reliably identified in all tumor-bearing animals. The growth pattern of the tumors resembled a spherical growth pattern, and the tumors showed a substantially uniform high-intensity signal. The results of the ADC and IVIM-related parameters for gemcitabine-treated group and saline-untreated group at day − 1, 1, 10 were shown in Table 2. As shown in Table 2 the values of ADC and D_{slow} in the entire tumor region were significantly increased in gemcitabine-treated group in contrast to saline-untreated group at day 1 ($1.88 \pm 0.34 \times 10^{-3}$ s/mm^2 vs $1.45 \pm 0.16 \times 10^{-3}$ s/mm^2, $P = 0.028$, and $1.74 \pm 0.29 \times 10^{-3}$ s/mm^2 vs $1.34 \pm 0.26 \times 10^{-3}$ s/mm^2, $P = 0.030$). No significant difference of pseudodiffusion coefficient D_{fast} and pseudodiffusion fraction f_p was found between the gemcitabine-treated group and saline-untreated group (Fig. 2).

Effects of gemcitabine on orthotopic pancreatic tumor growth

Gemcitabine (Met-Gem) can effectively inhibit the growth of pancreatic tumor compared to the saline-untreated group (Fig. 3). When tumor was excised from sacrificed mice after 4 weeks, the tumor volumes in gemcitabine-treated group were significantly lower than those in saline-untreated group at day 28 ($P = 0.0015$). Tumor in control group showed liquefaction necrosis at day 10 after treatment, while being more significant in gemcitabine group (Fig. 4).

Histological and immunohistochemistry assessment

The histology of orthotopic tumor tissues was examined using hematoxylin and eosin (H&E) staining. The tissues in the gemcitabine-treated group and saline-untreated group showed a typical histological appearance of pancreatic cancer (Fig. 5a). Boundaries between tumor tissue and surrounding normal tissue were unclear. Cancer cells were larger showing polygonal, spindle or irregular shape with cytoplasm lightly stained, the nucleus larger, the karyoplasmic ratio increased, and nucleoli were obvious. Tumor cells were arranged in a tubular or solid nest, no adenoid structure, consistent with the characteristics of poorly differentiated adenocarcinoma of the pancreas.

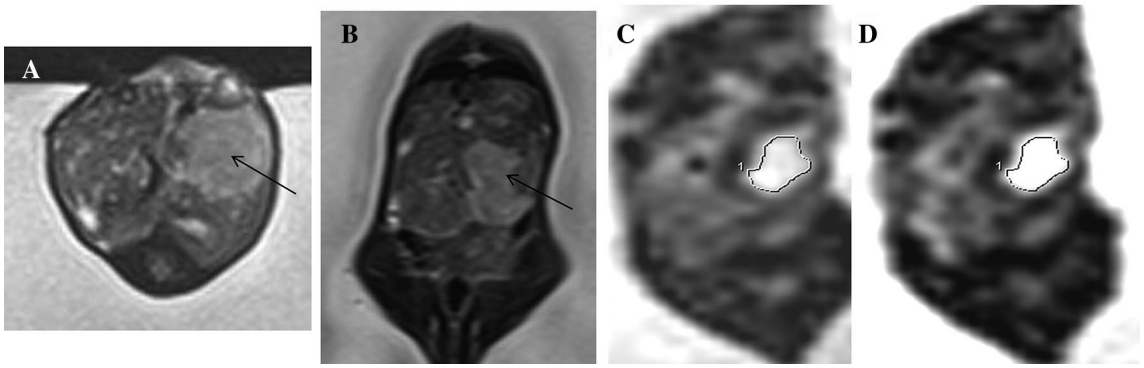

Fig. 1 T_2WI and parameter maps of one mouse. **a** Transversal T_2WI, **b** coronal T_2WI, tumor was indicated with black arrow. **c** ADC map, **d** D_{slow} map, an ROI was drawn around entire tumor area at the mid-level

Table 2 Mean (SD) of the diffusion parameters at − 1, 1, 10 day and *P* values between the two groups

	Day − 1			Day 1			Day 10		
	G	U	*P*	G	U	*P*	G	U	*P*
ADC, $\times 10^{-3}$ mn^2/s	1.66 (0.41)	1.31 (0.28)	0.121	1.88 (0.34)	1.45 (0.16)	0.028*	1.74 (0.14)	1.87 (0.14)	0.126
D_{slow}, $\times 10^{-3}$ mn^2/s	1.51 (0.33)	1.29 (0.40)	0.310	1.74 (0.29)	1.34 (0.26)	0.030*	1.65 (0.15)	1.76 (0.10)	0.186
D_{fast}, $\times 10^{-3}$ mn^2/s	17.93 (5.80)	17.02 (5.4)	0.688	15.08 (5.30)	14.17 (5.03)	0.629	19.12 (3.77)	16.61 (4.00)	0.249
f_p, %	13.00 (6.10)	12.62 (5.31)	0.861	10.32 (6.22)	12.13 (4.82)	0.383	11.39 (4.18)	10.40 (3.56)	0.625

G gemcitabine group, *U* saline-untreated group, $n = 6$/group; (*$P < 0.05$)

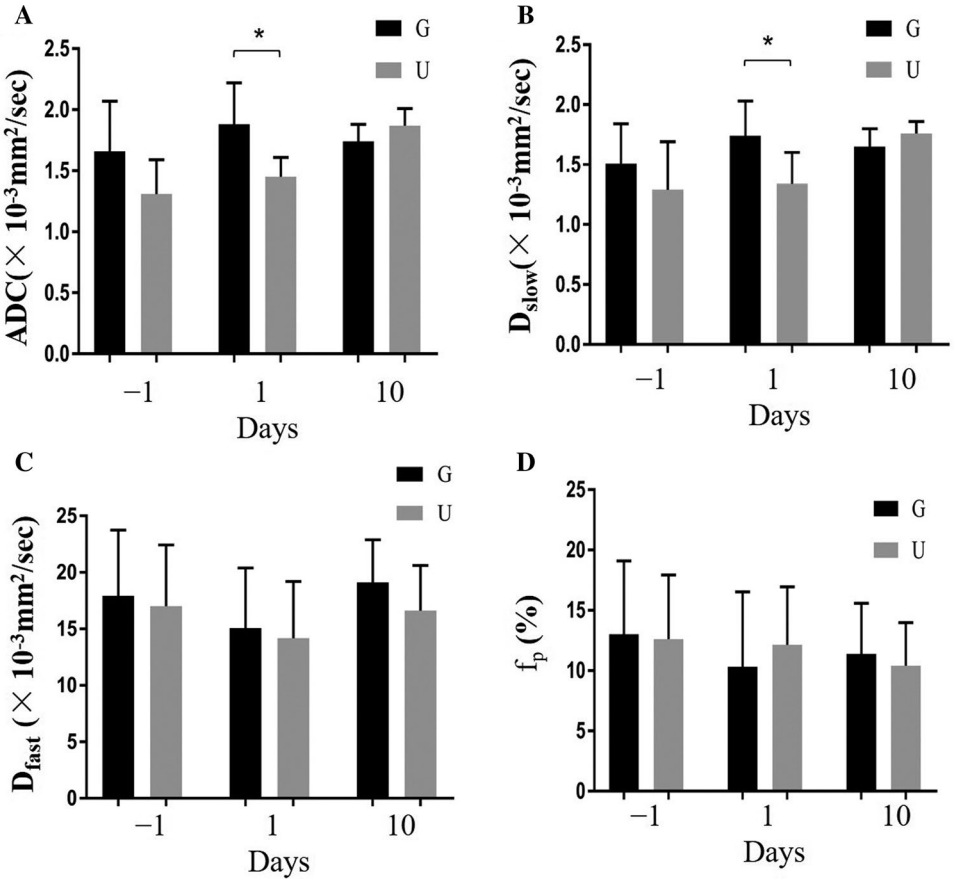

Fig. 2 The effect of treatment on ADC (**a**), D_{fast} (**b**), D_{slow} (**c**), and f_p (**d**) measured with DWI and IVIM. Statistical differences between groups were indicated by asterisks above bars (*P< 0.05). *G* gemcitabine group, *U* saline-untreated group

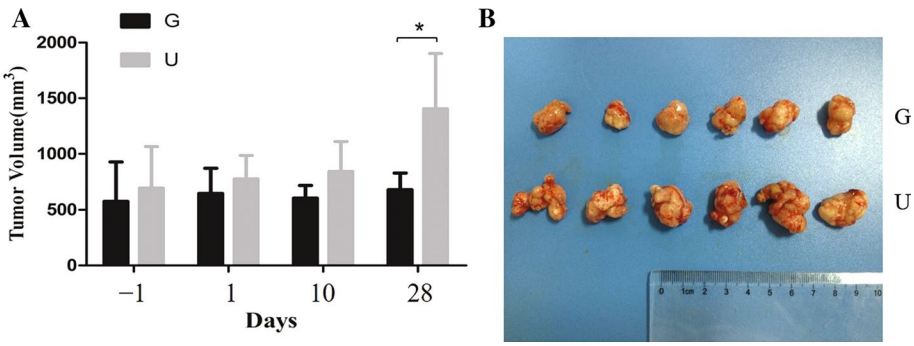

Fig. 3 Effects of gemcitabine on orthotopic pancreatic tumor growth. **a** Tumor volume size throughout the treatment schedule. **b** Gross morphorology of tumor at endpoint after gemcitabine (G) or saline (U) dosed. Statistical differences between groups were indicated by asterisks above bars (*P<0.05). *G* gemcitabine group, *U* saline-untreated group

Residual normal tissue remained around tumor. In addition, Fig. 5a showed representative microphotographs of Ki-67, TUNEL and CD31 staining of tumor tissues of two groups collected at day 28, with the proliferating cells, apoptosis cells and microvessel areas indicated with black arrows in each subfigure. Quantifications of proliferating cell (Ki-67 positive), apoptosis cell (TUNEL positive) and MVD of two groups presented in Fig. 5b–d, respectively. The apoptosis cell of saline-untreated group was significantly lower than that of gemcitabine-treated group ($P < 0.01$) (Fig. 5b), whereas the proliferating cell was significantly higher than that of gemcitabine-treated group ($P < 0.01$) (Fig. 5c). No significant differences in MVD were observed between the two groups (Fig. 5d).

Discussion and conclusion

As the first-line drugs approved for pancreatic cancer by FDA, gemcitabine can significantly improve the quality of life of patients with pancreatic cancer and prolong life span, and is the gold standard for the treatment of pancreatic cancer [3, 24]. However, in the clinical treatment, many patients with pancreatic cancer acquire resistance to chemotherapy

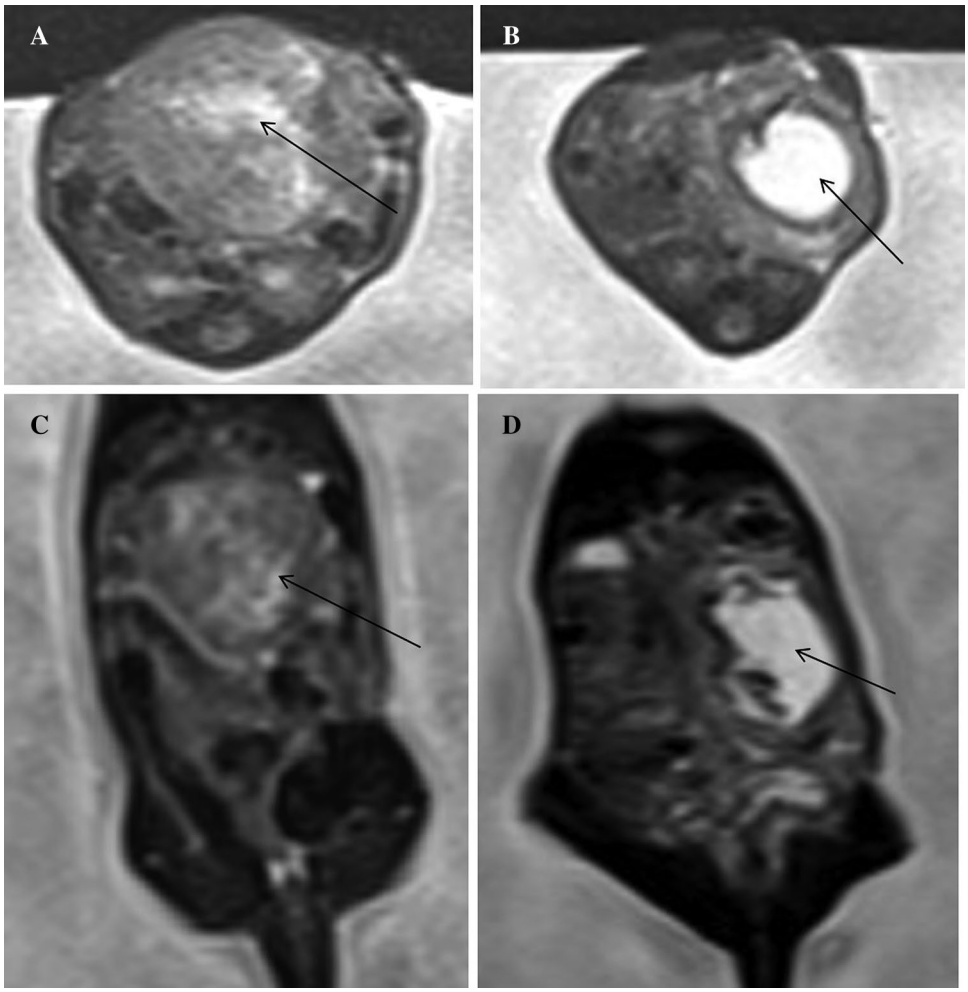

Fig. 4 T_2WI of tumor in mice at day 10 (**a**, **c**) and day 28 (**b**, **d**) after therapy with gemcitabine. Axial T_2WI (**a**, **b**), Coronal T_2WI (**c**, **d**), high intensity in the center of tumor (arrow) indicated necrosis and liquefaction

gemcitabine [25], which reduces the effects in the clinical application of gemcitabine, so it is important to evaluate the treatment of gemcitabine earlier.

As functional magnetic resonance imaging, diffusion-weighted imaging (DWI) can timely, accurately and reliably reflect the microscopic alterations of tissue composition and functional status of water exchange among the tissue components pathophysiologically by studying the microscopic movement of water molecules. The diffusion coefficient of DWI is called the apparent diffusion coefficient, reflecting the diffusion capacity of the tissue structure. Due to its large cell density, ADC value of solid tumor is smaller than that of normal tissue [26]. Recent studies have found signal attenuation is affected not only by the diffusion of water molecules but also by local capillary microcirculation when b value is lower [27, 28].

In this study, orthotropic model of pancreatic cancer in nude mice was established successfully. Compared with the subcutaneous model, orthotropic xenograft models are an ideal biological system for studying pancreatic cancer, as they can establish a human pancreatic cancer in its native site with the ability to expand relevance to drug evaluations. Referring to gemcitabine regimen in the clinical treatment, the value in the early assessment of efficacy was compared between IVIM-DWI and DWI. In this study, we used two different sequences instead of one sequence for IVIM and ADC acquisition. The reason is that we attempted to compare the parameters derived from the multiple-*b* IVIM sequence with the ADC derived from 3-*b* DWI sequence. The 3-*b* DWI sequence has its own advantage of shorter scanning time and less motion sensitivity. While IVIM sequence acquires more b values it needs longer scanning time and might be more motion-sensitive. Using ADC generated from the subset *b* values of the IVIM sequence might underestimate the performance of the conventional ADC. Thus, we use a separated sequence to acquired ADC. As can be seen from Table 2, the D_{slow} values and the ADC values were both statistically significant compared to the control group after 1 day of gemcitabine therapy. With rapid growth, tumor angiogenesis cannot keep up with the rate of tumor cell proliferation. There was liquefaction necrosis within the tumor

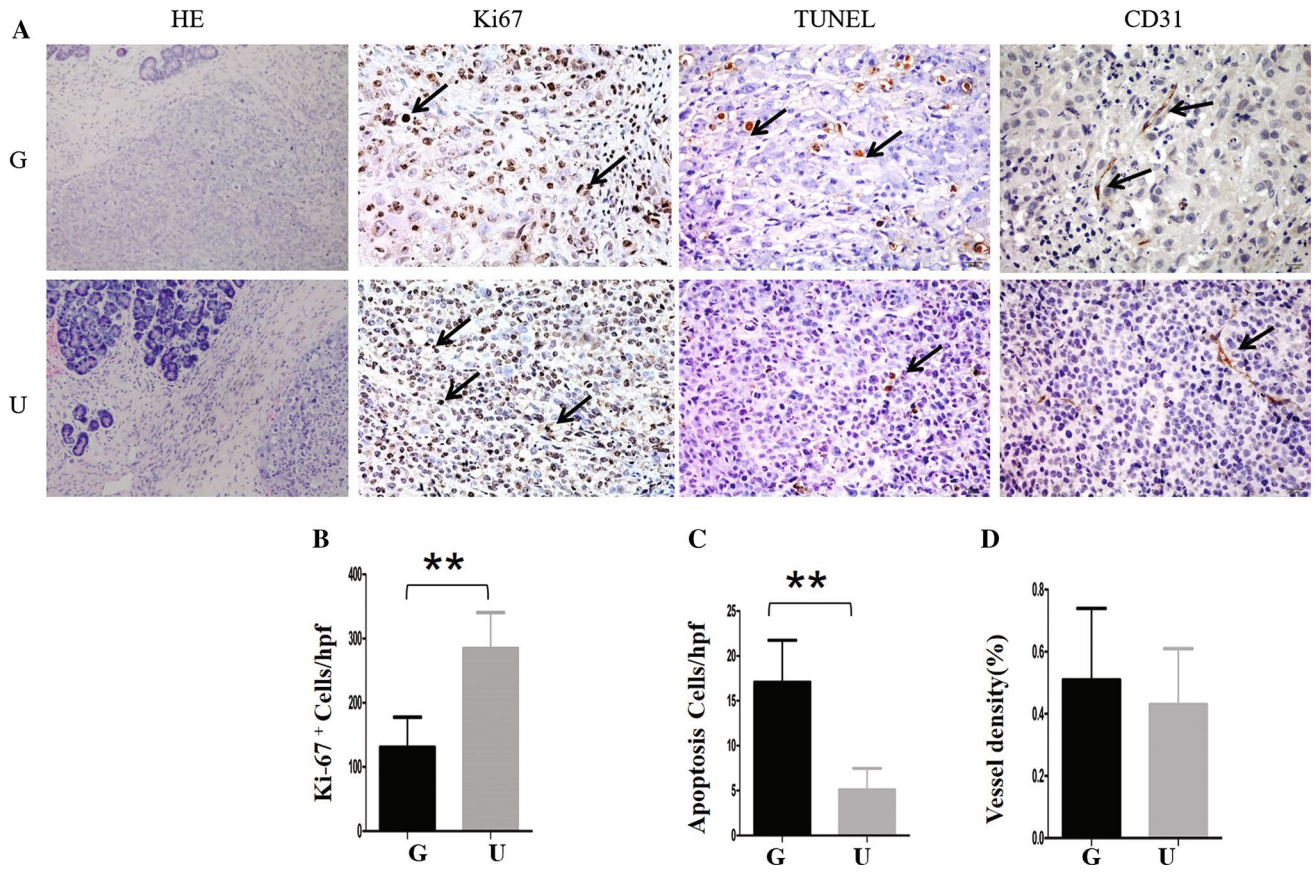

Fig. 5 Gemcitabine induces tumor responses through reducing proliferation and increasing apoptosis. **a** Representative microphotographs of HE (original magnification, ×200), Ki-67, TUNEL and CD31 staining (×400) in tumors dosed by Gemcitabine and saline. The proliferating cells, apoptosis cells and microvessel areas were indicated with black arrows in each row. **b–d** Proliferating (Ki-67 expressed) cell, apoptosis (TUNEL expressed) cell and microvessel (CD31 expressed) densities of gemcitabine and saline groups were presented; statistical differences between groups were indicated by asterisks above bars (**$P < 0.01$). *G* gemcitabine group, *U* saline-untreated group

formation and diffusion of water molecules enhanced in the corresponding region (Fig. 4). The increased diffusion of water molecules caused by the tumor necrosis is counteracted by the one caused by the intervention of gemcitabine. This may explain why the D_{slow} values and ADC values were not statistically significant at day 10 between two groups. Our results also showed that D_{fast} values and f_p values of gemcitabine-treated group were not statistically significant compared with the saline-untreated group at day 1 and day 10. Studies have found D_{fast} values and f_p values were positively correlated with MVD [29]. Gemcitabine is not an angiogenesis inhibitor and its main mechanism is to inhibit cell proliferation and induce cell apoptosis by interfering with DNA replication to cause DNA damage and block cell cycle progression, which was proved by tumor tissue immunohistochemistry indicators after the treatment period. Compared with saline-untreated group, cells in gemcitabine-treated group proliferated slower, apoptosis occured faster, and MVD changed less.

It is well known that when DWI is used on small experimental animals, the poor inhomogeneity of the magnetic field at the air–tissue interface produces severe susceptibility artefacts, with higher magnetic field intensity resulting in more severe artefacts [30, 31]. Some researchers have attempted examining animals using alginate moulding and ultrasonic coupling medium to improving signal intensity [32]. In this study, we choose a relatively simple and convenient method using 1.5 T MR, immersing experimental animals in liquid to isolate such air–tissue interface effects and achieving relatively satisfied results. Two points should be mentioned during the scanning process. First, scanning starts when the water is calm, the second is to keep the water temperature at 37.0 ± 0.2° C. The short scanning time in our plan, the maximum scanning time of the sequence is not more than 5 min, makes the two points feasible.

In conclusion, changes in ADC and D_{slow} value can be detected before gemcitabine treatment-induced reduction in tumor size. The earlier imaging technologies were used, the

less ADC and D_{slow} value were affected by tumor growth. Monitoring ADC and D_{slow} value could be important methods of assessing the early therapy efficacy of pancreatic cancer.

Acknowledgements This work was supported by the Medical and Technology Intercrossing Research Foundation of Shanghai Jiaotong University (YG2014QN07).

Compliance with ethical standards

Conflict of interest The authors declare that they have no conflict of interest.

Ethical approval Experiments were performed under protocols approved by the Animal Care Committee of Shanghai Jiao Tong University.

References

1. Siegel RL, Miller KD, Jemal A (2017) Cancer statistics, 2017. CA Cancer J Clin 67(1):7–30
2. Kamisawa T, Wood LD, Itoi T et al (2016) Pancreatic cancer. Lancet 388(10039):73–85
3. Burris HA 3rd, Moore MJ, Andersen J et al (1997) Improvements in survival and clinical benefit with gemcitabine as first-line therapy for patients with advanced pancreas cancer: a randomized trial. J Clin Oncol 15(6):2403–2413
4. Zhang XW, Ma YX, Sun Y et al (2017) Gemcitabine in combination with a second cytotoxic agent in the first-line treatment of locally advanced or metastatic pancreatic cancer: a systematic review and meta-analysis. Target Oncol 12(3):309–321
5. Panebianco C, Adamberg K, Jaagura M et al (2018) Influence of gemcitabine chemotherapy on the microbiota of pancreatic cancer xenografted mice. Cancer Chemother Pharmacol 81(4):773–782
6. Yapp DT, Wong MQ, Kyle AH et al (2016) The differential effects of metronomic gemcitabine and antiangiogenic treatment in patient-derived xenografts of pancreatic cancer: treatment effects on metabolism, vascular function, cell proliferation, and tumor growth. Angiogenesis 19(2):229–244
7. Zhang T, Zhang F, Meng Y et al (2013) Diffusion-weighted MRI monitoring of pancreatic cancer response to radiofrequency heat-enhanced intratumor chemotherapy. NMR Biomed 26(12):1762–1767
8. Galbán CJ, Ma B, Malyarenko D et al (2015) Multi-site clinical evaluation of DW-MRI as a treatment response metric for breast cancer patients undergoing neoadjuvant chemotherapy. PLoS One 10(3):e0122151
9. Woolf DK, Padhani AR, Makris A et al (2015) Magnetic resonance imaging, digital mammography, and sonography: tumor characteristics and tumor biology in primary setting. J Natl Cancer Inst Monogr 2015(51):15–20
10. Evelhoch JL, Gillies RJ, Karczmar GS et al (2000) Applications of magnetic resonance in model systems: cancer therapeutics. Neoplasia. 2:52–65
11. Padhani AR, Liu G, Koh DM et al (2009) Diffusion-weighted magnetic resonance imaging as a cancer biomarker: consensus and recommendations. Neoplasia. 11(2):102–125
12. Hejduk B, Bobek-Billewicz B, Rutkowski T et al (2017) Application of intravoxel incoherent motion (IVIM) model for differentiation between metastatic and non-metastatic head and neck lymph nodes. Pol J Radiol 82:506–510
13. Le Bihan D, Breton E, Lallemand D et al (1988) Separation of diffusion and perfusion in intravoxel incoherent motion MR imaging. Radiology 168(2):497–505
14. Doblas S, Wagner M, Leitao HS et al (2013) Determination of malignancy and characterization of hepatic tumor type with diffusion-weighted magnetic resonance imaging. Investig Radiol 10(48):1–7
15. Jerome NP, d'Arcy JA, Feiweier T et al (2016) Extended T2-IVIM model for correction of TE dependence of pseudo-diffusion volume fraction in clinical diffusion-weighted magnetic resonance imaging. Phys Med Biol 61(24):N667–N680
16. Cui Y, Zhang C, Li X et al (2015) Intravoxel incoherent motion diffusion-weighted magnetic resonance imaging for monitoring the early response to ZD6474 from nasopharyngeal carcinoma in nude mouse. Sci Rep 17(5):16389
17. Shirota N, Saito K, Sugimoto K et al (2016) Intravoxel incoherent motion MRI as a biomarker of sorafenib treatment for advanced hepatocellular carcinoma: a pilot study. Cancer Imaging 29(16):1
18. Pieper CC, Sprinkart AM, Meyer C et al (2016) Evaluation of a simplified intravoxel incoherent motion (IVIM) analysis of diffusion-weighted imaging for prediction of tumor size changes and imaging response in breast cancer liver metastases undergoing radioembolization: a retrospective single center analysis. Medicine (Baltimore) 95(14):e3275
19. Mini E, Nobili S, Caciagli B et al (2006) Cellular pharmacology of gemcitabine. Ann Oncol 17(Suppl 5):v7–v12
20. Tomayko MM, Reynolds CP (1989) Determination of subcutaneous tumor size in athymic (nude) mice. Cancer Chemother Pharmacol 24(3):148–154
21. Taouli B, Koh DM (2010) Diffusion-weighted MR imaging of the liver. Radiology 254:47–66
22. Luciani A, Vignaud M, Cavet JT et al (2008) Liver cirrhosis: intravoxel incoherent motion MR imaging – pilot study. Radiology 249(3):891–899
23. Mehta R, Kyshtoobayeva A, Kurosaki T et al (2001) Independent association of angiogenesis index with outcome in prostate cancer. Clin Cancer Res 7:81–88
24. Rothenberg ML, Moore MJ, Cripps MC et al (1996) A phase II trial of gemcitabine in patients with 5-FU-refractory pancreas cancer. Ann Oncol 7(4):347–353
25. Nakano Y, Tanno S, Koizumi K et al (2007) Gemcitabine chemoresistance and molecular markers associated with gemcitabine transport an metabolism in human pancreatic cancer cells. Br J Cancer 96(3):457–463
26. Yamada I, Aung W, Himeno Y, Nakagawa T, Shibuya H (1999) Diffusion coefficients in abdominal organs and hepatic lesions: evaluation with intravoxel incoherent motion echo-planar MR imaging. Radiology 210(3):617–623
27. Yoon JH, Lee JM, Yu MH, Kiefer B, Han JK, Choi BI (2014) Evaluation of hepatic focal lesions using diffusion-weighted MR imaging: comparison of apparent diffusion coefficient and intravoxel incoherent motion-derived parameters. J Magn Reson Imaging 39(2):276–285
28. Dijkstra H, Baron P, Kappert P, Oudkerk M, Sijens PE (2012) Effects of microperfusion in hepatic diffusion weighted imaging. Eur Radiol 22(4):891–899
29. Lee H-J, Rha SY, Chung YE, Shim HS, Kim YJ, Hur J, Hong YJ, Choi BW (2014) Tumor perfusion-related parameter of diffusion-weighted magnetic resonance imaging: correlation with histological microvessel density. Magn Reson Med 71(4):1554–1558
30. Chen F, De Keyzer F, Wang H, Vandecaveye V, Landuyt W, Bosmans H, Hermans R, Marchal G, Ni Y (2007) Diffusion weighted imaging in small rodents using clinical MRI scanners. Methods 43(1):12–20

31. Le Bihan D, Poupon C, Amadon A, Lethimonnier F (2006) Artifacts and pitfalls in diffusion MRI. J Magn Reson Imaging 24(3):478–488
32. Sun J, Zhang X-P, Li X-T, Tang L, Cui Y, Zhang X-Y, Sun Y-S (2015) Applicable apparent diffusion coefficient of an orthotopic mouse model of gastric cancer by improved clinical MRI diffusion weighted imaging. Sci Rep 4(1)